Physica A 611 (2023) 128421

Contents lists available at ScienceDirect

Physica A

journal homepage: www.elsevier.com/locate/physa

Isobaric heat capacity of carbon dioxide at critical pressure: Singular thermodynamic functions as multiply broken power laws

Roman Tomaschitz

Sechsschimmelgasse 1/21-22, A-1090 Vienna, Austria

ARTICLE INFO

Article history:
Received 21 July 2022
Received in revised form 17 November 2022
Available online 22 December 2022

Keywords:
Critical singularities and power-law scaling
Multiply broken power-law distributions and their Index functions
Isochoric and isobaric specific heat of single-component fluids
Isothermal and adiabatic compressibility and speed of sound
Isobaric and isentropic volume expansivity (expansion coefficient)

ABSTRACT

The isobaric CO_2 heat capacity at critical pressure is regressed in an extended temperature interval from the melting point at 216.6 K up to 2000 K. In the vicinity of the critical temperature $T_c = 304.13$ K, the calculated critical scaling exponent of the heat capacity is used to extrapolate the empirical data range into the power-law scaling regime. Closed-form representations of the high- and low-temperature branches of the isobaric CO_2 heat capacity are obtained by nonlinear least-squares fits of multiply broken power-law distributions, in which the calculated universal scaling exponent is implemented. The regressed broken power laws cover the temperature range from the melting point up to T_c and from T_c to CO_2 dissociation temperatures. Index functions representing the Log–Log slope of the heat capacity are used to quantify the crossover from the high- and low-temperature regimes to the critical power-law scaling regime. Even though the focus is on the isobaric heat capacity of a specific one-component fluid, the formalism is kept sufficiently general to be applicable to other thermodynamic functions with critical singularities and to multi-component mixtures.

1. Introduction

The aim of this paper is to extend empirical data sets of singular thermodynamic functions, such as the isobaric heat capacity at critical pressure or the isochoric heat capacity at critical density, into the critical scaling regime [1–5], where empirical data for fluids are scarce. We will substitute for missing data points by implementing calculated critical exponents in multiply broken power-law distributions. This will be explained at hand of a specific example, the isobaric heat capacity of carbon dioxide.

The second objective is to represent the full range of empirical data (e.g., from the melting point up to dissociation temperatures) and their extension into the critical scaling regime analytically. We will do this by using nonlinear least-squares regression of multiply broken power-law densities [6] in a temperature parametrization adapted to the critical scaling regime. Broken power-law densities are sufficiently flexible to model large data sets extending over several logarithmic decades, which is especially relevant for singular thermodynamic functions, where the power-law scaling regime is an extremely narrow interval centered at a critical-point parameter, the critical temperature in this paper. To describe the crossover from the low- and high-temperature regimes to the power-law scaling regime, we will employ Index functions [7], which represent the slope of the regressed thermodynamic function in double-logarithmic plots.

In Section 2.1, the multiplicative composition of broken power laws is explained, and temperature parametrizations are introduced that are suitable for critical-point singularities and also apply over the entire empirical temperature range,

E-mail address: tom@geminga.org.

https://doi.org/10.1016/j.physa.2022.128421
0378-4371/

from the melting point via the critical point to dissociation temperatures. The singular function studied in this paper is the isobaric heat capacity at critical pressure. Index functions are introduced in Section 2.2, and the least-squares regression of broken power laws is discussed in Section 2.3. The χ^2 functional for the fits is defined, and a systematic way to find initial values for the fitting parameters is pointed out, which are needed for the minimization of this nonlinear multiparameter functional.

In Section 3, the critical singularities of isochoric and isobaric heat capacities are sketched, including their relation to the critical power-law scaling of the isothermal and adiabatic compressibilities and isobaric and adiabatic expansion coefficients and the speed of sound. In particular, the critical scaling exponent of the isobaric heat capacity at critical pressure coincides with the scaling exponent of the isothermal compressibility on the critical isobar and is known, for the 3D Ising universality class, from model calculations (such as Monte Carlo simulations [8], conformal bootstrapping [9,10] and field-theoretic ε expansions [11], see also the reviews [1,2]). Special emphasis is given to the dependence of the scaling exponents on the chosen thermodynamic path to the critical point [12–14].

In Section 4, we model the isobaric CO_2 heat capacity at critical pressure with multiply broken power laws, using data points from Refs. [15,16] (that is, synthetic data generated from an empirical multiparameter equation of state for CO_2, cf. Ref. [17], which is based on a variety of experimental data sets). These data cover the interval from the melting point up to 2000 K and can be extended into the critical power-law scaling regime by means of the calculated scaling exponent. The broken power laws used for the least-squares regression of the high- and low-temperature branches of the heat capacity are specified in Sections 4.1 and 4.2. High- and low-temperature designations refer in this paper to $T > T_c$ and $T < T_c$, respectively.

In Section 5, the Index functions of the isobaric CO_2 heat capacity are calculated, describing the temperature evolution of the Log–Log slope of the high- and low-temperature branches of the heat capacity regressed in Section 4. These Index functions reach a constant limit value (identical with the scaling exponent) in the critical regime where the two branches of the heat capacity become simple power laws. In this way, one can estimate the temperature interval in which power-law scaling without perturbative scaling corrections applies, discounting impurities and gravitational rounding effects [3]. This is further discussed in the Conclusion, Section 6.

2. Thermodynamic functions as multiply broken power-law densities

2.1. Temperature parametrizations of functions with critical singularities

We will demonstrate that the temperature evolution of singular thermodynamic functions can accurately be modeled with broken power laws, which are defined as finite products, cf. Refs. [18–20],

$$p(\tau) = a_0 \tau^{\alpha_0} \prod_{k=1}^{n} \left(1 + (\tau/b_k)^{\beta_k/|\eta_k|}\right)^{\eta_k}, \tag{2.1}$$

with positive amplitudes a_0, b_k, positive exponents β_k, real exponent α_0 and positive or negative exponents η_k. It will also be convenient to write the amplitudes as $b_k = 10^{b_{10,k}}$, with real exponent $b_{10,k}$ as fitting parameter, especially when trying to find an initial guess for least-squares regression by visually fitting data sets in Log–Log representation. The distributions (2.1) are composed of power-law segments with smooth transitions, cf. Section 2.3.

The argument τ in (2.1) is a scaling variable related to the reduced temperature $t = T/T_c$ by $\tau = 1/(1-t)$ in the low-temperature regime $0 < t < 1$, $\tau > 1$, and by $\tau = 1/(t-1)$ at high temperature $t > 1$, $\tau > 0$. T_c denotes the critical temperature, and $\tau = 1/|T/T_c - 1|$.

Broken power-law densities of type (2.1) can be employed over the full empirical temperature range above the melting point. Especially the crossover to the critical scaling regime can be accurately represented by broken power laws, as they are particularly suitable for Log–Log representations of data sets extending over several logarithmic decades, cf. Sections 4 and 5.

Two types of double-logarithmic plots will be used. First, plots of a positive quantity $Q(t)$ in reduced temperature (abscissa Log t, ordinate Log $Q(t)$, where Log denotes the decadic logarithm). Data sets are labeled by $(t_i, Q_i)_{i=1,\ldots,N}$, $Q_i > 0$, where the $t_i = T_i/T_c$ are a discrete set of reduced temperatures.

To depict features of the quantity $Q(t)$ close to the critical point, it is convenient to use double-logarithmic plots in the scaling variable $\tau = 1/|t-1|$, $t = T/T_c$, which maps T_c to infinity. To this end, we split the data set $(t_i, Q_i)_{i=1,\ldots,N}$ into a low- and high-temperature component below and above T_c: $(t_i, Q_i)_{i=1,\ldots,N_{\rm low}}$ where $t_i < 1$, and $(t_i, Q_i)_{i=1,\ldots,N_{\rm high}}$ where $t_i > 1$ and $N = N_{\rm low} + N_{\rm high}$.

The low-temperature data set $(\tau_i, Q_i)_{i=1,\ldots,N_{\rm low}}$ with $\tau_i = 1/(1-t_i)$ can then be plotted in Log–Log representation, with abscissa Log τ_i and ordinate Log Q_i, where the τ_i range in the interval $1 < \tau < \infty$. Analogously for the high-temperature data points $(\tau_i, Q_i)_{i=1,\ldots,N_{\rm high}}$, with $\tau_i = 1/(t_i - 1)$ in the interval $0 < \tau < \infty$.

If $Q(\tau)$ is a broken power law density (2.1) regressed from the low-temperature data set $(\tau_i, Q_i)_{i=1,\ldots,N_{\rm low}}$ in the interval $1 < \tau < \infty$ or from the high-temperature data $(\tau_i, Q_i)_{i=1,\ldots,N_{\rm high}}$ in the interval $0 < \tau < \infty$, we can in either case substitute $\tau = 1/|t-1|$ into the respective regressed density to find $Q(\tau)$ as a function of reduced temperature $t = T/T_c$. (The shortcut $Q(t)$ will be used for $Q(1/|t-1|)$, where $Q(\tau)$ is a broken power law of type (2.1).)

The asymptotic limit of the distributions (2.1) is a simple power law,

$$p(\tau \to \infty) \sim B\tau^{\alpha_0+\sum_{k=1}^n \beta_k \mathrm{sign}(\eta_k)}, \quad B = a_0 \prod_{k=1}^n (1/b_k)^{\beta_k \mathrm{sign}(\eta_k)}. \tag{2.2}$$

Since the parametrization of $p(\tau)$ in reduced temperature $t = T/T_c$ is found by substituting $\tau = 1/|t-1|$, the limit (2.2) corresponds to $p(t \to 1) \sim B\,|t-1|^{-(\alpha_0+\sum_{k=1}^n \beta_k \mathrm{sign}(\eta_k))}$, which is singular if the power-law exponent in (2.2) is positive.

2.2. Index functions of broken power laws

Deviations from power-law scaling can be quantified by Index functionals. The Index of a multiply broken power-law distribution (2.1) is defined as, cf. Refs. [6,7],

$$\mathrm{Index}[p(\tau)] := \frac{p'(\tau)}{p(\tau)}\tau = \alpha_0 + \sum_{k=1}^n \mathrm{sign}(\eta_k)\beta_k \frac{(\tau/b_k)^{\beta_k/|\eta_k|}}{1+(\tau/b_k)^{\beta_k/|\eta_k|}}, \tag{2.3}$$

where the prime indicates differentiation. More generally, the Index of a composite function is

$$\mathrm{Index}[p(f(\tau))] = \frac{p'(f(\tau))}{p(f(\tau))} f'(\tau)\tau. \tag{2.4}$$

Thus, using the reciprocal scaling variable $\hat\tau = 1/\tau = |t-1|$ (also referred to as reduced temperature),

$$\mathrm{Index}[p(1/\hat\tau)] = -\mathrm{Index}[p(\tau)]|_{\tau=1/\hat\tau}. \tag{2.5}$$

The power laws (2.1) are form invariant with respect to the variable substitution $\tau = 1/\hat\tau$. That is, $p(1/\hat\tau)$ is also a broken power law that can be cast into the form (2.1). The τ parametrization mapping T_c to infinity rather than zero is more convenient for regression, cf. Section 2.3.

The Index represents the slope of $p(\tau)$ in Log–Log coordinates, $\mathrm{Index}[p(\tau)] = \mathrm{d}\log p(\tau)/\mathrm{d}\log\tau$. As power-law distributions of type (2.1) can stretch over several logarithmic decades, a Lin–Log (linear ordinate) representation of $\mathrm{Index}[p(\tau)]$ is usually most suitable. $\mathrm{Index}[p(\tau)]$ can undergo sign changes, of course. The Index of a simple power law is the power-law exponent, $\mathrm{Index}[A\tau^\alpha] = \alpha$, i.e. the slope of the straight line $A\tau^\alpha$ in Log–Log coordinates.

2.3. Least-squares regression of broken power laws

When minimizing the least-squares functional, it is preferable to write the broken power-law distribution (2.1) (with $b_k = 10^{b_{10,k}}$ and real exponents $b_{10,k}$) as

$$p(\tau) = a_0\tau^{\alpha_0} \prod_{k=1}^n (1+\hat b_k \tau^{\hat\beta_k})^{\hat\eta_k}, \tag{2.6}$$

where the parameters $\hat b_k$, $\hat\beta_k$, $\hat\eta_k$ are related to b_k, β_k, η_k in (2.1) by

$$\hat b_k = (10^{b_{10,k}})^{-\beta_k/|\eta_k|}, \hat\beta_k = \beta_k/|\eta_k|, \quad \hat\eta_k = \eta_k, \tag{2.7}$$

and inversely,

$$b_{10,k} = \mathrm{Log}(\hat b_k^{-1/\hat\beta_k}), \beta_k = \hat\beta_k|\hat\eta_k|, \quad \eta_k = \hat\eta_k. \tag{2.8}$$

Log denotes the decadic logarithm, and the exponents $\hat\beta_k$ and amplitudes $\hat b_k$ are positive.

The least-squares regression of the broken power laws for the heat capacity in Section 4 will be based on the χ^2 functional

$$\chi^2(a_0, \alpha_0, (\hat b_k, \hat\beta_k, \hat\eta_k)_{k=1,\ldots,n}) := \sum_{i=1}^N \frac{(p(\tau_i)-p_i)^2}{p_i^2}, \tag{2.9}$$

where the $(\tau_i, p_i)_{i=1,\ldots,N}$ denote a set of N data points, and $p(\tau; a_0, \alpha_0, (\hat b_k, \hat\beta_k, \hat\eta_k)_{k=1,\ldots,n})$ on the right-hand side of (2.9) is the broken power law (2.6).

When performing nonlinear least-squares fits with multiply broken power-law densities, it is essential to have a good initial guess for the parameters. To find that, one uses the parametrization in (2.1), rather than the rescaled parameters in (2.6). We assume the factors in (2.1) ordered by increasing amplitude $b_k < b_{k+1}$ and use a Log–Log plot of the data points $(\tau_i, p_i)_{i=1,\ldots,N}$. The distribution $p(\tau)$ in (2.1) consists of $n+1$ approximate power-law segments, $\propto \tau^{\alpha_0}$, $\tau^{\alpha_0+\beta_1\mathrm{sign}(\eta_1)}$, …, $\tau^{\alpha_0+\sum_{k=1}^n \beta_k\mathrm{sign}(\eta_k)}$, in the intervals $\tau \ll b_1$, $b_1 \ll \tau \ll b_2$, …, $b_n \ll \tau$, respectively. Simple power laws in Log–Log plots show as straight segments. The amplitudes b_k define the break points between the power-law segments and the

exponents η_k determine the extent of the transitional regions; if $|\eta_k| \ll 1$, this implies a narrow transitional interval with a sudden change of slope at b_k, cf. Ref. [6].

As mentioned, the factors in (2.1) are ordered by increasing amplitude, $b_1 < b_2 < \cdots < b_n$. In the range $\tau \ll b_k$, the factors defined by the amplitudes $b_k, b_{k+1}, \ldots, b_n$ are close to one and can be dropped. Therefore, one can obtain an initial guess by visually fitting the factors one by one, increasing the τ range in each step by adding the respective data points and the respective factor, which is facilitated by the fact that the above mentioned power-law segments appear as straight line segments in Log–Log plots.

3. Critical singularities of heat capacities, compressibility and volume expansivity

The isothermal compressibility is defined as $\kappa_T(T,P) = -V_{,P}/V = \rho_{,P}/\rho = 1/(\rho P_{,\rho})$, where $\rho(T,P)$ is the molar density, $V = 1/\rho(T,P)$ the molar volume and $P(T,\rho)$ the pressure (defined by an equation of state). Subscript commas followed by a variable indicate derivatives. The critical point parameters are denoted by (T_c, P_c, ρ_c, V_c). We will mainly use a (T,P) parametrization and the reduced quantities $t = T/T_c$, $p = P/P_c$.

If the critical point is approached along the critical isochore, $V(T,P) = V_c$, the isothermal compressibility scales as $\kappa_T \sim |t-1|^{-\gamma} \sim |p-1|^{-\gamma}$, with (3D Ising) scaling exponent $\gamma \approx 1.2371$, cf. e.g. Refs. [1–5]. To save notation, we drop the non-universal and path-dependent amplitude factors in the scaling relations [1,2,21]. The critical scaling exponents of carbon dioxide are in the 3D Ising universality class, to which most one-component fluids (including the quantum fluid hydrogen but not helium) belong. The most accurate 3D Ising exponents have been obtained with Monte Carlo simulations [8] and conformal bootstrapping [9].

The above power-law scaling also holds if the critical point is approached along the coexistence curve (of a single-component fluid), which terminates at the critical point in the (T,P) plane, or on a path tangential to the coexistence curve at the critical point. In contrast, if the path to the critical point is the critical isotherm $t = 1$ or the critical isobar $p = 1$, in which case the angle between the path and the direction of the coexistence curve at the critical point is finite, the isothermal compressibility scales as $\kappa_T \sim |p-1|^{-1+1/\delta}$ or $\kappa_T \sim |t-1|^{-1+1/\delta}$, with critical exponent $\delta = 4.7898$, cf. Refs. [12,22]. (The quoted critical exponents in this section are 3D Ising exponents.)

The scaling exponents of the isochoric heat capacity $C_V(T,P)$ likewise depend on the direction of the path relative to the coexistence curve at the critical point. Along the critical isochore or coexistence curve, $C_V(T,P)$ is weakly divergent, $C_V \sim |t-1|^{-\alpha} \sim |p-1|^{-\alpha}$, with critical exponent $\alpha = 0.1101$. If the path is the critical isotherm or critical isobar, the isochoric heat capacity scales as $C_V(T_c,P) \sim |p-1|^{-\alpha/(\beta\delta)}$ or $C_V(T,P_c) \sim |t-1|^{-\alpha/(\beta\delta)}$, where $\beta = 0.3264$ is the scaling exponent of the order parameter [12,22,23]. The critical exponents are related by $\alpha + 2\beta + \gamma = 2$ and $\alpha + \beta(1+\delta) = 2$. Derivations of the quoted power laws from critical scaling theory can be found in Refs. [24–27]. Thermodynamic paths to critical lines or critical surfaces in multi-component fluid mixtures are chosen with respect to coexistence hypersurfaces, cf. Refs. [12–14,28,29].

Isobaric (C_P) and isochoric (C_V) heat capacities are related by the identities $C_P - C_V = T(P_{,T})^2\rho_{,P}/\rho^2$ or $C_P - C_V = T(P_{,T})^2\kappa_T/\rho$, with density $\rho(T,P)$ and pressure $P(T,\rho)$ obtained from the equation of state. The isobaric expansion coefficient (volume expansivity) reads $\alpha_P = V_{,T}/V = P_{,T}\rho_{,P}/\rho = P_{,T}\kappa_T$, with molar volume $V(T,P)$ as above, so that $C_P = C_V + VT\alpha_P^2/\kappa_T$. See, for instance, Ref. [30] for a derivation of these identities. Since $P(T,\rho)$ and its temperature derivative $P_{,T}(T,\rho)$ are finite at the critical point, α_P and κ_T have the same scaling exponents.

As the scaling of the isochoric heat capacity is rather close to logarithmic, and since $C_P = C_V + T\alpha_P^2/(\rho\kappa_T)$, the leading singularity of the isobaric heat capacity C_P coincides with that of the isothermal compressibility and isobaric expansivity. In particular, $C_P(T,P) \sim |1-t|^{-\gamma}$ if the path to the critical point is the critical isochore, and $C_P(T,P_c) \sim |t-1|^{-1+1/\delta}$ at critical pressure [12,22].

The adiabatic (isentropic, reversible adiabatic) compressibility reads $\kappa_S = -V_{,P}(P,S)/V$, where $V(P,S)$ is the molar volume parametrized by pressure and entropy. κ_S is related to the isothermal compressibility by the heat capacity ratio, $\kappa_S = \kappa_T C_V/C_P$. The leading singularities of κ_T and C_P cancel each other out, so that κ_S scales like C_V.

The adiabatic expansion coefficient (isentropic expansivity) is defined as $\alpha_S = V_{,T}(T,S)/V$, where $V(T,S)$ is the molar volume parametrized by temperature and entropy. α_S is related to the adiabatic compressibility by $\alpha_S = 1/(P\kappa_S)$ and to the heat capacity ratio by $\alpha_S = (C_P/C_V)\rho P_{,\rho}/P$ (pressure $P(T,\rho)$), so that α_S scales inversely proportional to κ_S and C_V. Finally, the speed of sound υ_s is related to the adiabatic compressibility by $\upsilon_s = 1/\sqrt{\kappa_S\rho M}$, where M is the molar mass and ρ the molar density. Hence, $\upsilon_s \sim |1-t|^{\alpha/2}$ if the critical point is approached along the critical isochore, and $\upsilon_s \sim |1-t|^{\alpha/(2\beta\delta)}$ at critical pressure.

4. Modeling the isobaric CO_2 heat capacity at critical pressure with broken power laws

We split the temperature range into a low-temperature interval $[T_{\rm melt}, T_c]$, covering temperatures from the melting point to the critical point, and a high-temperature interval above T_c extending to 2000 K. In both intervals, broken power laws of type (2.1) will be used to model the isobaric CO_2 heat capacity at critical pressure ($P_c = 7.3773$ MPa), especially the crossover to the critical scaling regime, cf. Section 3.

Synthetic experimental data for the isobaric heat capacity of carbon dioxide, cf. Refs. [15,16], are plotted in Fig. 1, at critical pressure, from the melting temperature at $T_{\rm melt} = 216.6$ K up to 303.5 K (data points as filled squares) and from 305

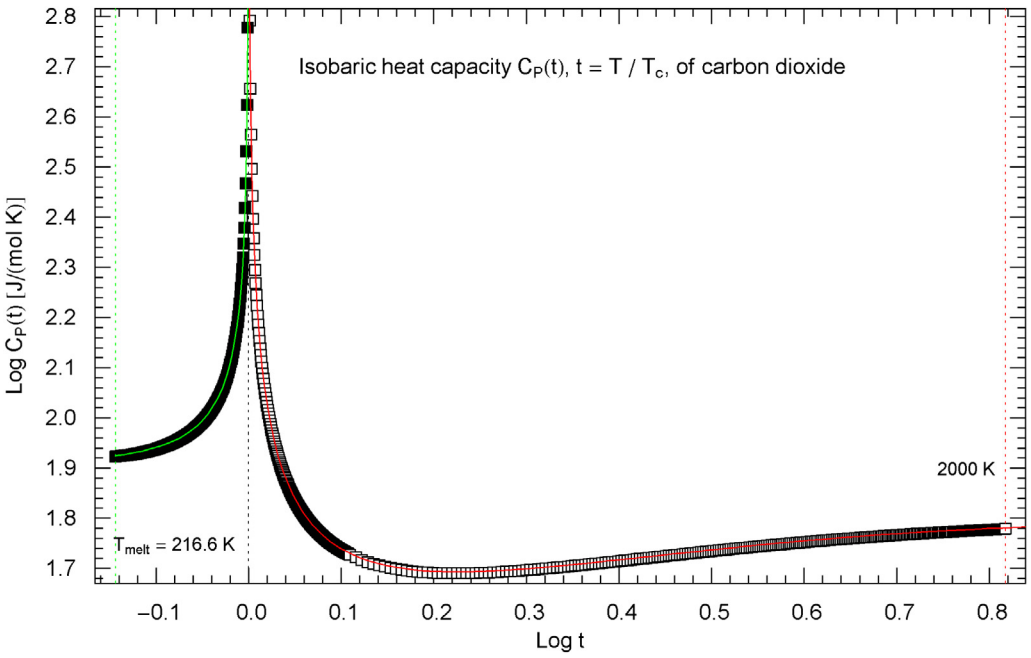

Fig. 1. Isobaric heat capacity of carbon dioxide at critical pressure. Data points from Refs. [15,16] (which are synthetic data based on a multiparameter equation of state [17]), covering the low-temperature interval from the melting temperature $T_{\rm melt} = 216.6\,$K up to 303.5 K (171 data points, filled squares) and the high-temperature range from 305 K up to 2000 K (440 data points, open squares). The critical temperature of carbon dioxide is $T_c = 304.13\,$K. Depicted is a Log–Log (decadic double-logarithmic) plot of the isobaric CO_2 heat capacity $C_P(t)$ (at the critical pressure of $P_c = 7.3773\,$MPa) versus reduced temperature $t = T/T_c$. The lower and upper temperature limits are indicated by the vertical green and red dotted lines. The red and green solid curves are the regressed high- and low-temperature branches of $C_P(t)$. The regression is discussed in Section 4 and Figs. 2 and 3, where temperature parametrizations more adapted to thermodynamic functions with critical singularities are used.

K up to 2000 K (open squares). The critical temperature of carbon dioxide is $T_c = 304.13\,$K. Even though a pronounced singularity emerges in Fig. 1, the indicated temperature ranges are still separated from the power-law scaling regime, which is a narrow interval centered at T_c where $C_P \sim A_\pm\,|1 - T/T_c|^{1/\delta-1}$ with critical exponent $\delta = 4.7898$ holds, cf. Section 3. (The amplitudes A_+ and A_- refer to $T > T_c$ and $T < T_c$, respectively.) Ideal power-law scaling only occurs at temperatures differing from T_c by a tiny fraction of 1 K. Therefore, a plot of the heat capacity $C_P(t)$ in reduced temperature $t = T/T_c$ as in Fig. 1 is unsuitable to visualize the scaling regime and the crossover to the data points depicted in Fig. 1.

The same data sets [15,16] are plotted double-logarithmically in Figs. 2 and 3 in different parametrizations. The low-temperature ($T_{\rm melt} < T < T_c$) data points are depicted as filled squares and the high-temperature ($T_c < T < 2000\,$K) data as open squares, like in Fig. 1. In Fig. 2, the heat capacity $C_P(\tau)$ is parametrized with the scaling variable $\tau = 1/\,|t-1|$, $t = T/T_c$, cf. after (2.1). The least-squares fits described below are performed in this parametrization. In Fig. 3, the regressed heat capacity is reparametrized with the inverted variable, i.e. with reduced temperature $\hat\tau = 1/\tau = |1-t|$. In this section, least-squares regression will be used to derive an analytic representation (2.1) of the isobaric heat capacity at critical pressure, which covers the temperature range from $T_{\rm melt}$ up to 2000 K, including the scaling regime above and below T_c where simple power-law scaling occurs.

4.1. Isobaric heat capacity at critical pressure in the high-temperature regime

The data sets $(\tau_i, C_{P,i})$, $\tau_i = 1/(T_i/T_c - 1)$, in the high-temperature regime comprise 440 data points in the interval between 305 K and 2000 K (open squares in Fig. 2, taken from Refs. [15,16]). The least-squares fit of the heat capacity component above T_c is performed with the broken power law, cf. Section 2,

$$C_P(\tau) = a_0\frac{1}{(1+(\tau/b_2)^{\beta_2/\eta_2})^{\eta_2}}(1+(\tau/b_3)^{\beta_3/\eta_3})^{\eta_3}, \tag{4.1}$$

with positive amplitudes a_0, b_k and positive exponents β_k, η_k as parameters. Scaling theory predicts the isobaric heat capacity at critical pressure to scale as $C_P(\tau\to\infty) \sim A_+\tau^{1-1/\delta}$, with exponent $\delta = 4.7898$, cf. Section 3. This can be used to eliminate one fitting parameter in (4.1), by substituting $\beta_3 = 1 - 1/\delta + \beta_1 - \beta_2$, with $1 - 1/\delta = 0.7912$. The scaling amplitude is obtained from the regressed parameters, $A_+ = a_0 b_1^{\beta_1}/(b_2^{\beta_2} b_3^{\beta_3})$, cf. the caption to Table 1. The asymptotic power-law scaling $A_+\tau^{1-1/\delta}$ is depicted as red dashed straight line in Fig. 2.

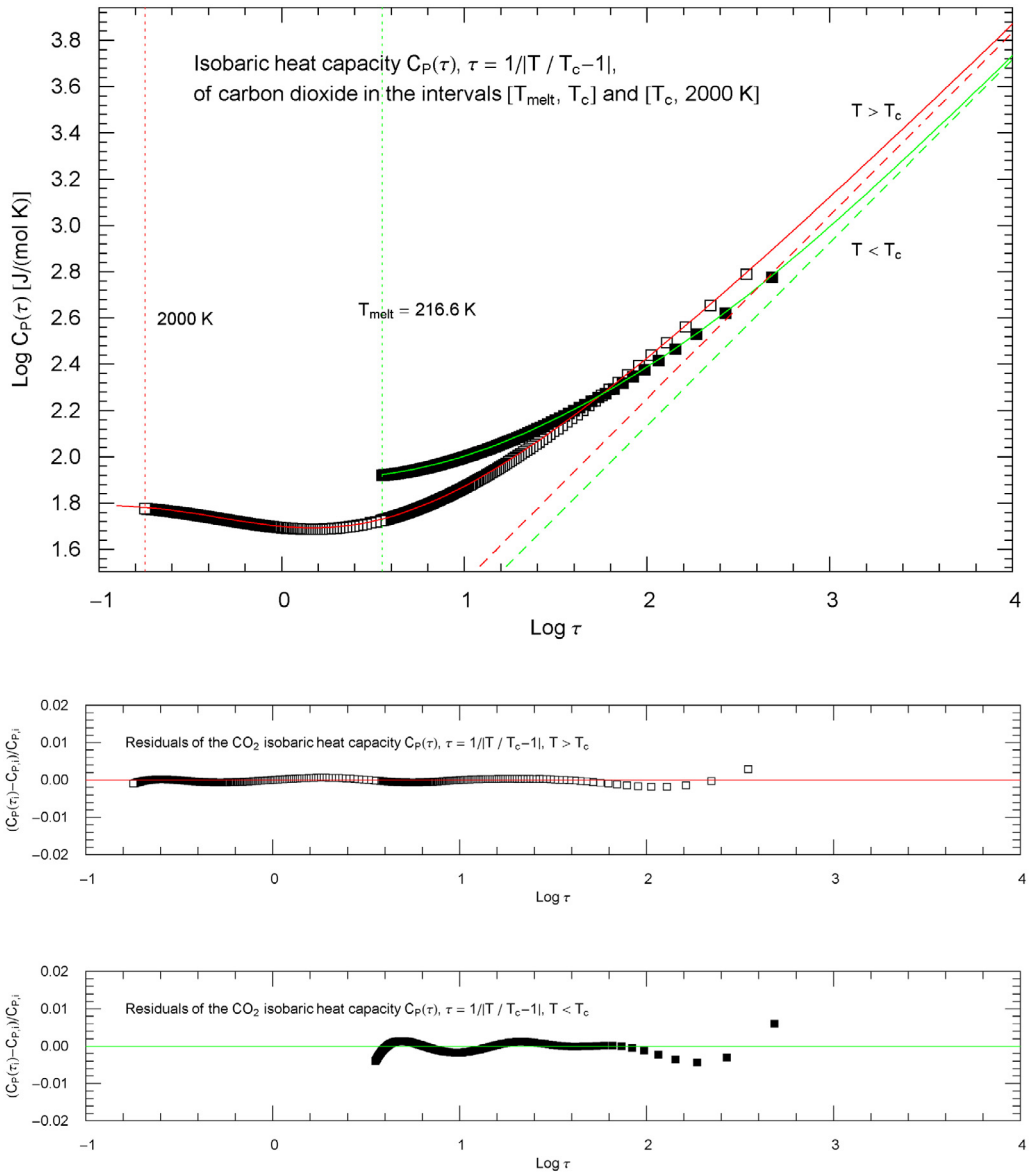

Fig. 2. Isobaric heat capacity $C_P(\tau)$ of carbon dioxide at critical pressure, parametrized with the scaling variable $\tau = 1/|T/T_c - 1|$. The open and filled squares are data points from Refs. [15,16], the same as in Fig. 1. In the high-temperature regime, $T/T_c > 1$, $\tau = 1/(T/T_c - 1)$, the data points are depicted as open squares and in the low-temperature regime, $T/T_c < 1$, $\tau = 1/(1 - T/T_c)$, as filled squares. In this τ parametrization, the critical temperature is mapped to infinity, $\tau(T_c) = \infty$. The filled squares cover the interval [T_{melt}, 303.5 K] and the open squares the interval [305 K, 2000 K]. The red and green solid curves depict the high- and low-temperature heat capacities $C_P(\tau)$ in (4.1) (for $T > T_c$) and (4.3) (for $T < T_c$) regressed from the depicted data sets, cf. Tables 1 and 2 and Section 4. The χ^2 functional used for the regression is stated in (4.2); residuals of the least-squares fits of the high- and low-temperature branches (4.1) and (4.3) of $C_P(\tau)$ are shown in the lower panels, indicating relative errors below one percent. The red and green dashed lines represent simple power laws, $A_\pm \tau^{1-1/\delta}$, which are the asymptotes of the high- and low-temperature components of $C_P(\tau)$, respectively, cf. Section 4 and the captions of Tables 1 and 2. These straight lines have a Log–Log slope of $1 - 1/\delta = 0.7912$, which is the critical exponent of the isobaric heat capacity at critical pressure of a fluid in the 3D Ising universality class such as CO_2, cf. Section 3.

The least-squares functional to be minimized is

$$\chi^2(a_0, (b_k, \beta_k, \eta_k)_{k=1,2,3}) = \sum_{i=1}^{N} \frac{(C_P(\tau_i) - C_{P,i})^2}{C_{P,i}^2}, \tag{4.2}$$

where $(\tau_i, C_{P,i})_{i=1,\ldots,N}$, $N = 440$, are the data points mentioned above, and $C_P(\tau; a_0, (b_k, \beta_k, \eta_k)_{k=1,2,3})$ is the broken power law (4.1). The fitting parameters $a_0, (b_k, \beta_k, \eta_k)_{k=1,2,3}$ are recorded in Table 1. (The decadic logarithm $\mathrm{Log}\, b_k$ rather than

Table 1
Fitting parameters of the high-temperature ($T > T_c$) isobaric heat capacity of carbon dioxide at critical pressure $P_c = 7.3773$ MPa. The nonlinear least-squares fit to data sets specified in Section 4 is performed with the broken power law, cf. (4.1),
$C_P(\tau) = a_0(1+(\tau/b_1)^{\beta_1/\eta_1})^{-\eta_1}(1+(\tau/b_2)^{\beta_2/\eta_2})^{\eta_2}(1+(\tau/b_3)^{\beta_3/\eta_3})^{\eta_3}$,
parametrized with the scaling variable (reciprocal reduced temperature) $\tau = 1/(T/T_c - 1)$, $T > T_c$. Because of the critical power-law scaling, $C_P(\tau\to\infty) \sim A_+\tau^{1-1/\delta}$, where $1-1/\delta = 0.7912$ is the calculated critical exponent of the isobaric heat capacity at P_c, one of the fitting parameters can be eliminated, e.g., by substituting $\beta_3 = 1 - 1/\delta + \beta_1 - \beta_2$. The least-squares functional is stated in (4.2), and the regression is explained in Section 4.1, see also Section 2.3. The data points and the regressed heat capacity $C_P(\tau)$ in the high-temperature interval between T_c and 2000 K are depicted in Fig. 2 (open squares, red solid curve), including a residual plot. The regressed parameters $a_0, (b_k, \beta_k, \eta_k)_{k=1,2,3}$ of $C_P(\tau)$ are listed in this table. $\mathrm{Log}\, b_k$ denotes the decadic logarithm of the amplitudes b_k. Also recorded are the minimum of the least-squares functional χ^2 and the degrees of freedom of the fit (dof: number N of data points minus number of fitting parameters). The amplitude of the critical power law $C_P \sim A_+\tau^{1-1/\delta}$ is inferred from the regressed parameters, $A_+ = a_0 b_1^{\beta_1}/(b_2^{\beta_2} b_3^{\beta_3}) = 4.660$ J/(mol K).

a_0 [J/(mol K)]	$\mathrm{Log}\, b_1$	β_1	η_1	$\mathrm{Log}\, b_2$	β_2	η_2
53.2889	– 0.561891	1.21177	0.999673	0.00220725	1.76494	2.22004
$\mathrm{Log}\, b_3$	β_3	η_3	χ^2			dof
1.56900	0.238027	0.66239	7.55×10^{-5}			440 – 9

Table 2
Parameters of the low-temperature ($T_{\mathrm{melt}} \le T \le T_c$) branch of the isobaric heat capacity of carbon dioxide at critical pressure. The least-squares regression is performed with the broken power law, cf. (4.3),
$C_P(\tau) = a_0(1+(\tau/b_1)^{\beta_1/\eta_1})^{\eta_1}(1+(\tau/b_2)^{\beta_2/\eta_2})^{\eta_2}$,
parametrized with the scaling variable $\tau = 1/(1 - T/T_c)$, $T < T_c$. The asymptotic critical power-law scaling of the low-temperature branch, $C_P(\tau\to\infty) \sim A_-\tau^{1-1/\delta}$, with calculated exponent $\delta = 4.7898$ can be implemented by identifying $\beta_2 = 1 - 1/\delta - \beta_1$. The least-squares functional is assembled analogous to χ^2 in (4.2), and the regression is explained in Section 4.2. The data points and the regressed low-temperature heat capacity $C_P(\tau)$ including a residual plot of the fit are depicted in Fig. 2 (filled squares, green solid curve). The regressed $C_P(\tau)$ is applicable in the interval between the melting point (where $C_P(\tau)$ has a discontinuity) and T_c. The parameters $a_0, (b_k, \beta_k, \eta_k)_{k=1,2}$ of $C_P(\tau)$ are listed in this table, $\mathrm{Log}\, b_k$ denoting the decadic logarithm of b_k. Also recorded are the minimum of the least-squares functional χ^2 and the degrees of freedom (dof) of the fit, cf. the caption of Table 1. The critical scaling amplitude A_- is calculated from the regressed parameters as $A_- = a_0/(b_1^{\beta_1} b_2^{\beta_2}) = 3.563$ J/(mol K).

a_0 [J/(mol K)]	$\mathrm{Log}\, b_1$	β_1	η_1	$\mathrm{Log}\, b_2$	β_2	η_2
74.3358	0.808595	0.194948	0.0933792	1.94849	0.596252	0.893048
χ^2						dof
3.33×10^{-4}						171 – 6

the amplitude b_k is listed in this table.) The regressed high-temperature ($T > T_c$) branch (4.1) of the isobaric heat capacity $C_P(\tau)$ is depicted in Fig. 2 as red solid curve.

Remark. For the minimization of χ^2, it is essential to have a good initial guess of the fitting parameters. A systematic way to find initial values for multiply broken power-law distributions of type (2.1) (or (4.1) as a special case) is outlined in Section 2.3, cf. after (2.9). Once an initial guess for $C_P(\tau)$ has been found, it is also advisable to simplify the parametrization in (4.1) when minimizing the χ^2 functional, by introducing rescaled fitting parameters $\hat{b}_k$, $\hat{\beta}_k$, $\hat{\eta}_k$ defined in (2.6)–(2.8).

In Fig. 1, the isobaric heat capacity is parametrized with reduced temperature $t = T/T_c$. The red solid curve in this figure is the regressed high-temperature $C_P(\tau)$ in (4.1) with $\tau = 1/(t-1)$ substituted (shortcut $C_P(t)$).

Fig. 3 shows the same data sets as Fig. 2, also in decadic Log–Log representation, but now parametrized with reduced temperature $\hat{\tau} = 1/\tau = |1-t|$. The depicted data points are $(\hat{\tau}_i, C_{P,i})$, with $\hat{\tau}_i = |1 - T_i/T_c|$ and $C_{P,i}$ as in Fig. 2. Apart from this reparametrization and an extended temperature range toward T_c, Fig. 3 is otherwise analogous to Fig. 2, the main difference being that the critical temperature T_c is mapped to zero ($\hat{\tau}(T_c) = 0$) instead of infinity. The asymptotic power laws $A_\pm\hat{\tau}^{1/\delta-1}$ of the isobaric heat capacity in the scaling regime above and below T_c (red and green dashed lines in Fig. 3) have a negative slope $1/\delta - 1 = -0.7912$ in $\hat{\tau}$ parametrization. The red solid curve in Fig. 3 is a plot of the high-temperature heat capacity parametrized with $\hat{\tau} = t - 1$, that is $C_P(\tau)$ in (4.1) with $\tau = 1/\hat{\tau}$ substituted (shortcut $C_P(\hat{\tau})$).

4.2. Low-temperature interval between melting point and critical temperature

The broken power-law density defining the low-temperature branch of the isobaric heat capacity at critical pressure in the interval $[T_{\mathrm{melt}}, T_c]$ is obtained analogously to the high-temperature counterpart in Section 4.1. The data set $(\tau_i, C_{P,i})$ used for the regression in this interval comprises 171 data points between $T_{\mathrm{melt}} = 216.6$ K and 303.5 K (filled squares in Fig. 2, cf. Refs. [15,16]).

The least-squares fit of the low-temperature isobaric heat capacity is performed with the broken power law, cf. (2.1),

$$C_P(\tau) = a_0(1+(\tau/b_1)^{\beta_1/\eta_1})^{\eta_1}(1+(\tau/b_2)^{\beta_2/\eta_2})^{\eta_2}, \tag{4.3}$$

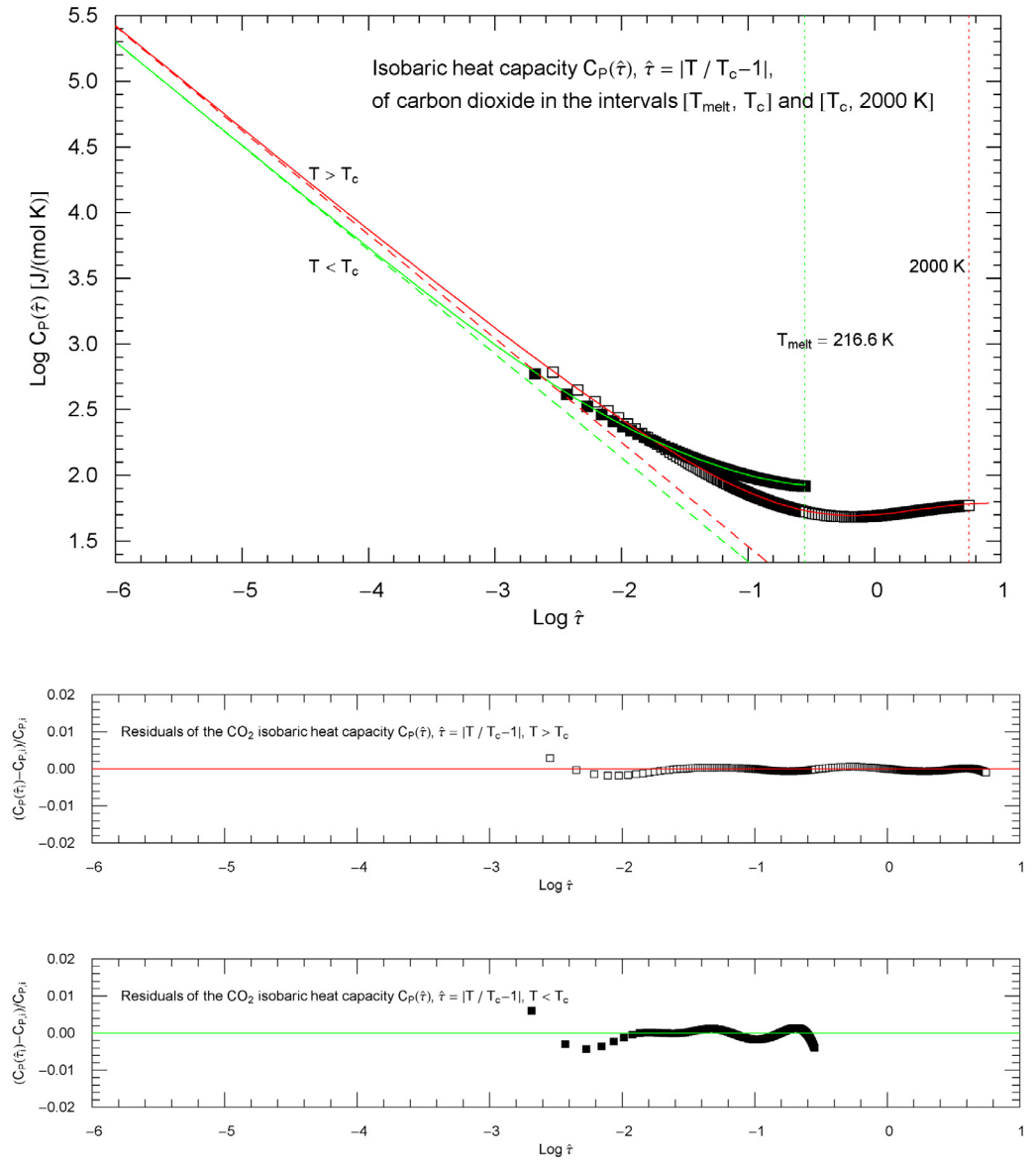

Fig. 3. Isobaric heat capacity $C_P(\hat\tau)$ of carbon dioxide at critical pressure $P_c = 7.3773$ MPa, parametrized with reduced temperature $\hat\tau = |T/T_c - 1|$. In the high-temperature regime, $T/T_c > 1$, the data points are depicted as open squares and in the low-temperature regime, $T/T_c < 1$, as filled squares. The red and green solid curves show the broken power laws (4.1) and (4.3) (with $\tau = 1/\hat\tau$ substituted and parameters in Tables 1 and 2) representing the high- and low-temperature branches of the CO_2 heat capacity $C_P(\hat\tau)$. Apart from this reparametrization with the reciprocal variable $\hat\tau$ and an extended temperature interval, the data points, regressed heat-capacity curves (4.1) and (4.3) and the residuals of the fits depicted in the lower panels are the same as in Fig. 2. The red and green dashed straight lines show the critical power laws $A_\pm \hat\tau^{1/\delta-1}$ (with exponent $\delta = 4.7898$ and amplitudes $A_\pm$ stated in the captions of Tables 1 and 2) asymptotic to the high- and low-temperature branches of $C_P(\hat\tau)$, cf. Section 4. The green and red dotted vertical lines indicate the melting temperature and the upper experimental temperature limit of 2000 K, where thermal dissociation into CO and O_2 sets in.

where the amplitudes a_0, b_k and exponents β_k, η_k are positive. To implement the asymptotic critical power-law scaling $C_P(\tau \to \infty) \sim A_- \tau^{1-1/\delta}$, cf. Section 3, we substitute $\beta_2 = 1 - 1/\delta - \beta_1$ in (4.3). The asymptote $A_- \tau^{1-1/\delta}$ with amplitude $A_- = a_0/(b_1^{\beta_1} b_2^{\beta_2})$ is shown as green dashed line in Fig. 2; the regressed amplitude A_- is stated in the caption of Table 2.

The least-squares functional $\chi^2(a_0, (b_k, \beta_k, \eta_k)_{k=1,2})$ reads as in (4.2), now assembled with $C_P(\tau)$ in (4.3) and data points $(\tau_i, C_{P,i})_{i=1,\ldots,N}$, $\tau_i = 1/(1-t_i)$, $N = 171$, as indicated above. The fitting parameters a_0, $(b_k, \beta_k, \eta_k)_{k=1,2}$ are listed in Table 2. The regressed low-temperature $C_P(\tau)$ in (4.3) is shown in Fig. 2 as green solid curve.

In Fig. 1, the low-temperature heat capacity (4.3) is plotted as a function of reduced temperature $t = T/T_c$, $C_P(\tau = 1/(1-t))$ (shortcut $C_P(t)$, green solid curve in Fig. 1). In Fig. 3, the green solid curve depicts $C_P(\tau)$ in (4.3) with $\tau = 1/\hat\tau$

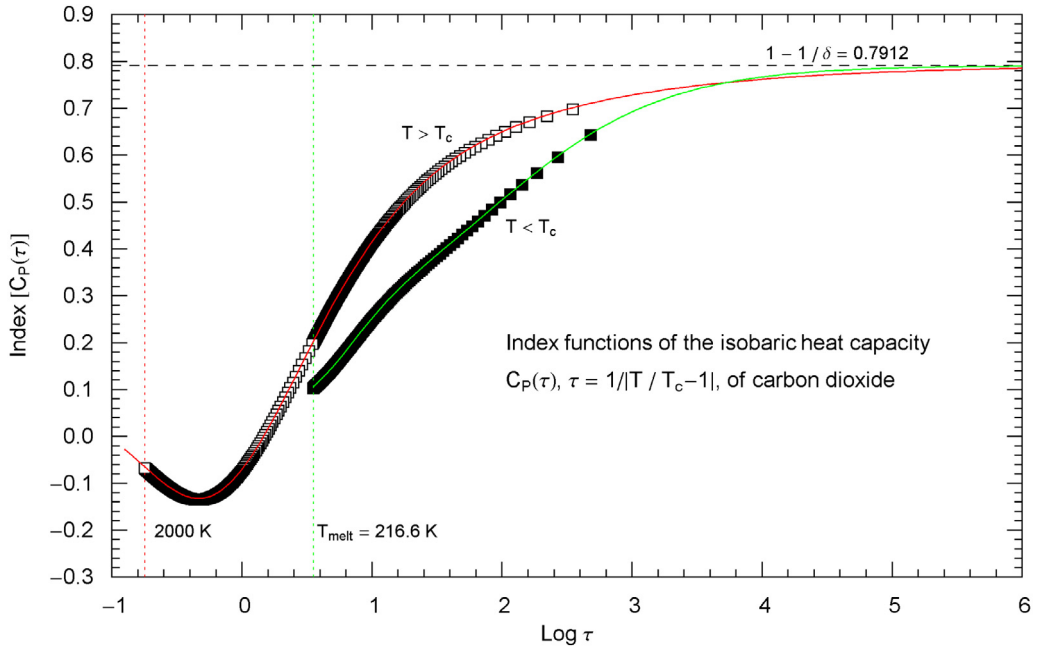

Fig. 4. Index functions of the isobaric heat capacity of carbon dioxide at critical pressure, parametrized with scaling variable $\tau = 1/|T/T_c - 1|$. The red and green solid curves depict the Log–Log slope $\mathrm{Index}[C_P(\tau)] = \mathrm{d}\log C_P(\tau)/\mathrm{d}\log\tau$ of the high- and low-temperature branches of the heat capacity $C_P(\tau)$, cf. Sections 2.2 and 5. (The latter are depicted in Fig. 2, covering the intervals $[T_c, 2000\,\mathrm{K}]$ and $[T_{\mathrm{melt}}, T_c]$.) The plotted high- and low-temperature Index functions $\mathrm{Index}[C_P(\tau)]$ are stated in (5.1) (red solid curve, $\tau = 1/(T/T_c - 1)$, $T > T_c$) and (5.2) (green solid curve, $\tau = 1/(1 - T/T_c)$, $T < T_c$), with parameters recorded in Tables 1 and 2. The open squares along the high-temperature Index curve and the filled squares along the low-temperature Index curve correspond to the heat capacity data points depicted in Fig. 2 by the same markers, see also after (5.1) and (5.2). The vertical red and green dotted lines indicate the experimental temperature limits T_{melt} and 2000 K. The scaling exponent $1 - 1/\delta = 0.7912$ of the isobaric heat capacity at critical pressure is indicated by the black dashed horizontal line, which is the asymptote of the depicted Index curves, i.e. the constant $\tau \to \infty$ limit of $\mathrm{Index}[C_P(\tau)]$ in (5.1) and (5.2). This horizontal line is also a plot of the constant Index function (Log–Log slope) of the asymptotic critical power laws $A_\pm \tau^{1-1/\delta}$ in Fig. 2.

substituted (shortcut $C_P(\hat\tau)$), double-logarithmically plotted against the inverted scaling variable $\hat\tau = 1/\tau = 1 - t$, $t = T/T_c < 1$. The green dashed straight line in Fig. 3 is the power-law asymptote $A_- \hat\tau^{1/\delta - 1}$.

The Log–Log slope of the $T > T_c$ and $T < T_c$ heat-capacity branches (red and green solid curves, respectively) in the temperature intervals covered by data points (open and filled squares in Figs. 2 and 3) is noticeably smaller than the calculated scaling exponent $1 - 1/\delta = 0.7912$ of the 3D Ising universality class, as will be quantified in Section 5 by means of Index functions. The slope of 0.7912 is represented in Fig. 2 by the red and green dashed straight lines, which are asymptotes of the high- and low-temperature branches of $C_P(\tau)$. In the reduced temperature parametrization $\hat\tau = 1/\tau = 1 - t$ of Fig. 3, the slope of the depicted red and green asymptotes of $C_P(\hat\tau)$ is -0.7912.

5. Index functions of the CO_2 heat capacity

5.1. Index function of the high-temperature isobaric heat capacity at critical pressure

Fig. 4 shows the Index function (cf. Section 2.2) of the regressed high-temperature heat capacity $C_P(\tau)$ in (4.1),

$$\mathrm{Index}[C_P(\tau)] = -\beta_1 \frac{(\tau/b_1)^{\beta_1/\eta_1}}{1+(\tau/b_1)^{\beta_1/\eta_1}} + \beta_2 \frac{(\tau/b_2)^{\beta_2/\eta_2}}{1+(\tau/b_2)^{\beta_2/\eta_2}} + \beta_3 \frac{(\tau/b_3)^{\beta_3/\eta_3}}{1+(\tau/b_3)^{\beta_3/\eta_3}}. \tag{5.1}$$

To better relate Fig. 4 to Fig. 2, we have plotted data points $(\tau_i, \mathrm{Index}[C_P(\tau_i)])_{i=1,\ldots,N}$ (open squares) on the (red solid) Index curve, using the abscissas τ_i of the data points $(\tau_i, C_{P,i})_{i=1,\ldots,N}$ in Fig. 2 (also indicated by open squares).

The red solid curve in Fig. 5 depicts the Index function $\mathrm{Index}[C_P(\hat\tau)]$ of the reparametrized high-temperature heat capacity $C_P(\hat\tau)$ in Fig. 3. Plotted in Fig. 5 is $\mathrm{Index}[C_P(\hat\tau)]$ versus $\mathrm{Log}\,\hat\tau$, where $\hat\tau = t - 1$, $t = T/T_c > 1$ is the reduced temperature. The Index function $\mathrm{Index}[C_P(\hat\tau)]$ is obtained from $\mathrm{Index}[C_P(\tau)]$ in (5.1) by substituting $\tau = 1/\hat\tau$ and an overall sign change, cf. (2.5). The open squares in Fig. 5 depict data points $(\hat\tau_i, \mathrm{Index}[C_P(\hat\tau_i)])_{i=1,\ldots,N}$ on the Index curve with abscissas $\hat\tau_i$ from the corresponding high-temperature data points $(\hat\tau_i, C_{P,i})_{i=1,\ldots,N}$ in Fig. 3.

$\mathrm{Index}[C_P(\hat\tau)]$ gives the Log–Log slope of the high-temperature heat capacity curve $C_P(\hat\tau)$ in Fig. 3. By the way, Log–Log slopes have also been used to define temperature-dependent effective critical exponents of thermodynamic functions in Refs. [31–33]; see also Ref. [7] and references therein for the use of Index functions in other research fields.

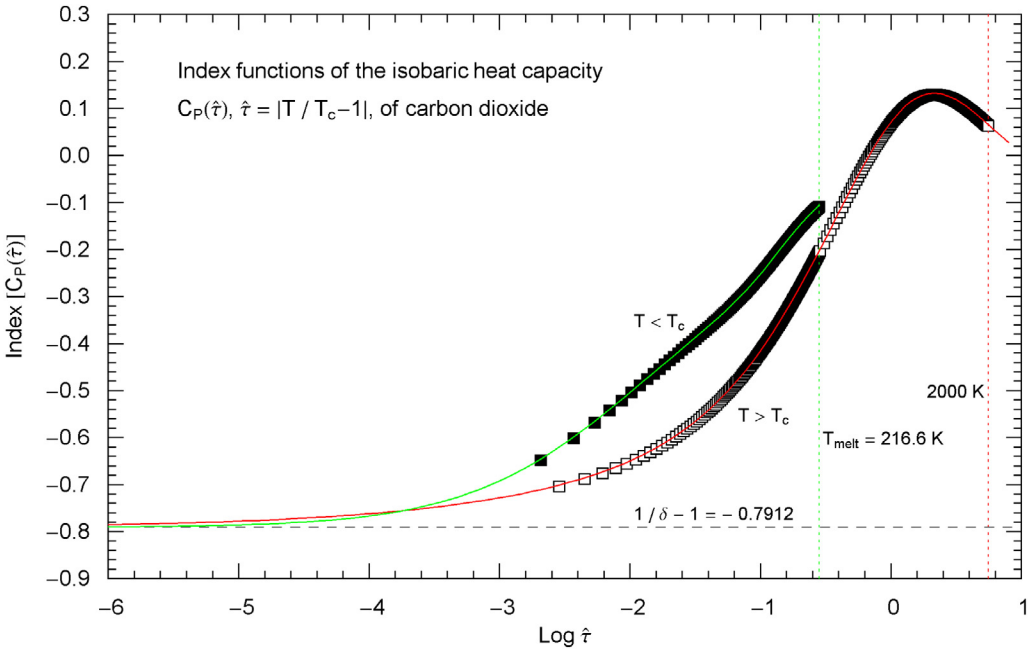

Fig. 5. Index functions of the isobaric heat capacity of carbon dioxide at critical pressure, parametrized with reduced temperature $\hat\tau = |T/T_c - 1|$. The red and green solid curves are plots of the Index functions Index$[C_P(\hat\tau)]$ of the high- and low-temperature branches of the heat capacity $C_P(\hat\tau)$ in Fig. 3. The (red solid) high-temperature curve Index$[C_P(\hat\tau)]$ is a plot of $-$Index$[C_P(\tau)]$ in (5.1) with $\tau = 1/\hat\tau$ substituted, and the (green solid) low-temperature curve is obtained from (5.2) by the same substitution and an overall sign change, cf. (2.5). The open and filled squares plotted along the Index curves correspond to the heat capacity data points depicted in Fig. 3. The vertical red and green dotted lines indicate the experimental temperature limits. The scaling exponent $1-1/\delta = 0.7912$ of the isobaric heat capacity at critical pressure is indicated by the black dashed horizontal line, which is the asymptote of the depicted high- and low-temperature Index functions Index$[C_P(\hat\tau)]$ for $\hat\tau \to 0$. This horizontal line also depicts the constant Index function of the critical power laws $A_\pm \hat\tau^{1/\delta-1}$ asymptotic to the high- and low-temperature heat capacity curves in Fig. 3.

5.2. Low-temperature Index function

The reasoning in this section is analogous to the high-temperature counterpart in Section 5.1. The Index function of the regressed low-temperature heat capacity $C_P(\tau)$ in (4.3) covering the interval $[T_{\rm melt}, T_c]$ is depicted in Fig. 4 as green solid curve,

$$\text{Index}[C_P(\tau)] = \beta_1 \frac{(\tau/b_1)^{\beta_1/\eta_1}}{1+(\tau/b_1)^{\beta_1/\eta_1}} + \beta_2 \frac{(\tau/b_2)^{\beta_2/\eta_2}}{1+(\tau/b_2)^{\beta_2/\eta_2}}, \tag{5.2}$$

which represents the Log–Log slope of the low-temperature ($T < T_c$) branch of $C_P(\tau)$ in Fig. 2. Along the (green solid) Index curve in Fig. 4, we have indicated data points $(\tau_i, \text{Index}[C_P(\tau_i)])_{i=1,\ldots,N}$ (filled squares) with the same abscissas τ_i as the low-temperature data points $(\tau_i, C_{P,i})_{i=1,\ldots,N}$ in Fig. 2.

Fig. 5 shows the Index function Index$[C_P(\hat\tau)]$ (green solid curve) of the reparametrized low-temperature heat capacity $C_P(\hat\tau)$ in Fig. 3 (which is $C_P(\tau)$ in (4.3) with $\tau = 1/\hat\tau$ substituted), depicting the Log–Log slope of $C_P(\hat\tau)$. The scaling variable in this case is the reduced temperature $\hat\tau = 1 - t$, $t = T/T_c < 1$. Index$[C_P(\hat\tau)]$ is obtained from Index$[C_P(\tau)]$ in (5.2) by substituting $\tau = 1/\hat\tau$ and a sign change, cf. (2.5). The filled squares in Fig. 5 are data points $(\hat\tau_i, \text{Index}[C_P(\hat\tau_i)])_{i=1,\ldots,N}$ on the Index curve with abscissas $\hat\tau_i$ stemming from the low-temperature data points $(\hat\tau_i, C_{P,i})_{i=1,\ldots,N}$ in Fig. 3.

Outside the empirical data range (open and filled squares in Figs. 1–5), the Index functions in Fig. 4 do not exceed 0.7 (or -0.7 in Fig. 5). The slope of $1 - 1/\delta = 0.7912$ exhibiting the critical power-law scaling of the isobaric heat capacity is only reached at temperatures extremely close to $T_c = 304.13$ K, in the interval $|T/T_c - 1| \le 10^{-5}$ (see Figs. 4 and 5), far outside the temperature range of the depicted data points [15,16]. The regressed broken power laws in (4.1) and (4.3) extrapolate the empirical data range into the scaling regime, by making use of the calculated critical exponent $\delta = 4.7898$ of the 3D Ising universality class, cf. Section 4.

6. Conclusion

The topic of this paper was the phenomenological analytic modeling of thermodynamic functions with critical singularities. Specifically, empirical data sets covering the temperature range from the melting point to the high-temperature regime were used for the regression of the isobaric CO_2 heat capacity at critical pressure. The power-law

scaling regime of the isobaric heat capacity is manifested in a narrow interval centered at the critical temperature, separated from the available data points [15,16] by about two orders of magnitude in reduced temperature, as illustrated by Index functions in Figs. 4 and 5.

As for other thermodynamic functions, such as the isochoric heat capacity or the isothermal compressibility, measurements in the critical region were reported for a limited number of one-component fluids. For instance, the scaling exponents and amplitudes of the isochoric heat capacity at critical density and/or the isothermal compressibility on the critical isochore were measured for hydrogen [34], nitrogen [35], water [36–38], carbon dioxide [39–42], neon [35], xenon [43], sulfur hexafluoride (SF_6) [40,44–47], fluoroform (CHF_3) [48], and also helium [3,49], the latter being in a different universality class. See also Refs. [14,15,28,29,50,51] for experiments on the critical scaling properties of binary and ternary mixtures. Multiply broken power-law densities as defined in (4.1) are quite adaptable and can be used for all thermodynamic quantities enumerated in Section 3, provided that one can find data sets covering an extended temperature or pressure range, cf. e.g. Refs. [15–17].

Given the scarcity of experimental data in the power-law scaling regime, the next best option is to extrapolate the data range analytically by means of calculated critical exponents. In Section 4, we used the calculated exponent δ of the 3D Ising universality class to extend the empirical data range of the isobaric CO_2 heat capacity at critical pressure into the power-law scaling regime. This was done by way of closed-form multiply broken power laws, replacing the truncated ascending series expansions and range-shrinking methods around the critical temperature customarily used in experimental papers, cf. e.g. Refs. [28,34,35,43–46,48–52].

Truncated series with one or two correction terms and different series coefficients above and below T_c (for instance, $C_P = A_\pm \hat\tau^{1/\delta-1}(1+a_\pm\hat\tau^\Delta+\cdots)$, where $\Delta = 0.523$ is a universal correction-to-scaling exponent [8–10]) are efficient in the extended scaling regime, typically within an interval $\hat\tau = |T/T_c - 1| < 0.01$ or 0.1. These series are used to experimentally infer critical amplitudes and occasionally also critical indices [50,51], but they are not suitable for the global modeling of thermodynamic functions over the complete temperature range from the melting point to dissociation temperatures, which is the topic of this paper. The broken power laws (4.1) and (4.3) are non-perturbative and applicable over the entire temperature range, and the critical scaling is implemented by means of calculated critical indices. That is, critical exponents are input and the regression is not a test of scaling predictions but based on them.

In the case of the isobaric CO_2 heat capacity at critical pressure, the empirical data sets from Refs. [15,16] do not extend into the $|T/T_c - 1| < 10^{-3}$ range, cf. Fig. 3, whereas ideal power-law scaling without correction terms only occurs in the $|T/T_c - 1| < 10^{-5}$ interval, cf. Fig. 5, where we invoked the calculated critical exponent. The data sets from Refs. [15,16] cover temperatures from the melting point to 2000 K, except in the vicinity of T_c. These are synthetic precision data, with relative error below one percent, obtained from a multiparameter equation of state [17] and available in machine-readable format. The relative errors of the least-squares fits of the broken power laws are also below one percent, as can be seen from the residual panels of Figs. 2 and 3. The regressed broken power laws of the high- and low-temperature branches of the CO_2 heat capacity are also depicted in these figures, parametrized with the scaling variable $\tau = 1/|T/T_c - 1|$ or the reciprocal variable $\hat\tau = |T/T_c - 1|$. The latter is the standard reduced temperature parametrization in critical scaling theory, but the inverse τ is more suitable for the least-squares regression of multiply broken power laws, cf. Section 2.3. In τ parametrization, the critical temperature is mapped to infinity, $\tau(T \to T_c) \to \infty$, cf. Figs. 2 and 4, and in $\hat\tau$ parametrization to zero as in Figs. 3 and 5, otherwise these reciprocal parametrizations are equivalent.

Figs. 4 and 5 show the Index functions (cf. Sections 2.2 and 5) of the high- and low-temperature branches of the isobaric CO_2 heat capacity at critical pressure, which represent the Log–Log slope of the broken power-law densities (4.1) and (4.3) in Figs. 2 and 3. Within the empirical data range (from Refs. [15,16], indicated by the open and filled squares in Figs. 2 and 3), the Log–Log slope of the heat capacity curves barely reaches a value of 0.7. The critical power-law scaling regime, where the slope coincides with the scaling exponent $1 - 1/\delta = 0.7912$, is separated from the empirical data range by at least two logarithmic decades in reduced temperature, as illustrated by Fig. 5. A limitation of heat capacity measurements in the scaling regime is gravitational density stratification resulting in a rounding of power-law slopes, cf. e.g. Refs. [35,40,53]. Gravitational rounding of the experimental slopes already sets in at about $|T/T_c - 1| \sim 10^{-4}$, cf. Ref. [53], and the ideal power-law scaling interval is by one order narrower, as pointed out above.

To summarize, empirical data are used in a temperature range where their relative error is estimated to be below one percent [15,16], and calculated exponents accurate to several decimal digits [8,9] are used in the critical regime, and this suffices to obtain a non-perturbative analytic closed-form representation of the heat capacity covering the temperature range from the melting point to dissociation temperatures including the critical power-law scaling regime. This is done with nonlinear multiparameter fits of broken power laws, cf. Sections 2.1 and 4, which are uniformly accurate over the complete temperature range, as can be seen from the residual plots in Figs. 2 and 3.

Declaration of competing interest

The author declares that he has no known competing financial interests or personal relationships that could have appeared to influence the work reported in this paper.

Data availability

The URLs of the data sources are indicated in the reference list, cf. Refs. [15,16].

Acknowledgment

My thanks to an anonymous referee for suggestions, questions and useful comments, which have greatly helped to improve an earlier draft of this paper.

References

[1] A. Pelissetto, E. Vicari, Critical phenomena and renormalization-group theory, Phys. Rep. 368 (2002) 549.
[2] V. Privman, P.C. Hohenberg, A. Aharony, Universal critical-point amplitude relations, in: C. Domb, J.L. Lebowitz (Eds.), Phase Transitions and Critical Phenomena, Vol. 14, Academic Press, New York, 1991.
[3] M. Barmatz, I. Hahn, J.A. Lipa, R.V. Duncan, Critical phenomena in microgravity: Past, present, and future, Rev. Modern Phys. 79 (2007) 1.
[4] M.E. Fisher, The theory of equilibrium critical phenomena, Rep. Progr. Phys. 30 (1967) 615.
[5] M. Vicentini-Missoni, J.M.H. Levelt Sengers, M.S. Green, Scaling analysis of thermodynamic properties in the critical region of fluids, J. Res. Natl. Bur. Stand. A Phys. Chem. 73A (1969) 563.
[6] R. Tomaschitz, Multiply broken power-law densities as survival functions: An alternative to Pareto and lognormal fits, Physica A 541 (2020) 123188.
[7] R. Tomaschitz, Modeling electrical resistivity and particle fluxes with multiply broken power-law distributions, Eur. Phys. J. Plus 136 (2021) 629.
[8] M. Hasenbusch, Finite size scaling study of lattice models in the three-dimensional Ising universality class, Phys. Rev. B 82 (2010) 174433.
[9] S. El-Showk, M.F. Paulos, D. Poland, S. Rychkov, D. Simmons-Duffin, A. Vichi, Solving the 3d Ising model with the conformal bootstrap II. c-Minimization and precise critical exponents, J. Stat. Phys. 157 (2014) 869.
[10] P.H. Lundow, I.A. Campbell, The Ising universality class in dimension three: Corrections to scaling, Physica A (2018) 40.
[11] J. Zinn-Justin, Precise determination of critical exponents and equation of state by field theory methods, Phys. Rep. 344 (2001) 159.
[12] R.B. Griffiths, J.C. Wheeler, Critical points in multicomponent systems, Phys. Rev. A 2 (1970) 1047.
[13] E. Bloemen, J. Thoen, W. Van Dael, The specific heat anomaly in triethylamine–heavy water near the critical solution point, J. Chem. Phys. 73 (1980) 4628.
[14] E. Bloemen, J. Thoen, W. Van Dael, The specific heat anomaly in some ternary liquid mixtures near a critical solution point, J. Chem. Phys. 75 (1981) 1488.
[15] E.W. Lemmon, I.H. Bell, M.L. Huber, M.O. McLinden, NIST Standard Reference Database 23, Reference Fluid Thermodynamic and Transport Properties-REFPROP, Version 10.0, National Institute of Standards and Technology, Gaithersburg, 2018, http://dx.doi.org/10.18434/T4/1502528.
[16] E.W. Lemmon, M.O. McLinden, D.G. Friend, Thermophysical properties of fluid systems, in: P.J. Linstrom, W.G. Mallard (Eds.), NIST Chemistry WebBook, NIST Standard Reference Database 69, 2022, https://webbook.nist.gov/chemistry/fluid/.
[17] R. Span, W. Wagner, A new equation of state for carbon dioxide covering the fluid region from the triple-point temperature to 1100 K at pressures up to 800 MPa, J. Phys. Chem. Ref. Data 25 (1996) 1509.
[18] R. Tomaschitz, Phenomenological high-pressure equation of state for nitrogen, methane, methanol, carbon dioxide, and helium, Int. J. Thermophys. 43 (2022) 130.
[19] R. Tomaschitz, Multiparameter equation of state for classical and quantum fluids, J. Supercrit. Fluids 181 (2022) 105491.
[20] R. Tomaschitz, Thermodynamics of lattice vibrations in non-cubic crystals: the zinc structure revisited, Acta Crystallogr. A 77 (2021) 420.
[21] M. Hasenbusch, Universal amplitude ratios in the three-dimensional Ising universality class, Phys. Rev. B 82 (2010) 174434.
[22] J. Stephenson, On the critical region of a simple fluid. II. Scaling-law equation of state, J. Chem. Phys. 54 (1971) 895.
[23] Y.C. Kim, M.E. Fisher, Singular coexistence-curve diameters: Experiments and simulations, Chem. Phys. Lett. 414 (2005) 185.
[24] R.B. Griffiths, Thermodynamic functions for fluids and ferromagnets near the critical point, Phys. Rev. 158 (1967) 176.
[25] M. Barmatz, P.C. Hohenberg, A. Kornblit, Scaled-equation-of-state analysis of the specific heat in fluids and magnets near critical point, Phys. Rev. B 12 (1975) 1947.
[26] A. Aharony, P.C. Hohenberg, Universal relations among thermodynamic critical amplitudes, Phys. Rev. B 13 (1976) 3081.
[27] J.V. Sengers, J.M.H. Levelt Sengers, Critical phenomena in classical fluids, in: C.A. Croxton (Ed.), Progress in Liquid Physics, Wiley, New York, 1978.
[28] P. Losada-Pérez, C.A. Cerdeiriña, J. Thoen, Asymmetric liquid-liquid criticality in the ideal volumetric mixing approximation, J. Chem. Thermodyn. 128 (2019) 356.
[29] P. Losada-Pérez, C.S.P. Tripathi, J. Leys, C. Glorieux, J. Thoen, Large heat capacity anomaly near the consolute point of the binary mixture nitromethane and 3-pentanol, J. Chem. Phys. 134 (2011) 044505.
[30] E. Whalley, The compression of liquids, in: B. Le Neindre, B. Vodar (Eds.), Experimental Thermodynamics, Vol. 2: Experimental Thermodynamics of Non-Reacting Fluids, Butterworths, London, 1975.
[31] J.S. Kouvel, M.E. Fisher, Detailed magnetic behavior of nickel near its Curie point, Phys. Rev. 136 (1964) A1626.
[32] J.V. Sengers, J.G. Shanks, Experimental critical-exponent values for fluids, J. Stat. Phys. 137 (2009) 857.
[33] P. Losada-Pérez, C.A. Cerdeiriña, Coexisting densities and critical asymmetry between gas and liquid, J. Chem. Thermodyn. 109 (2017) 56.
[34] J.R. de Bruyn, D.A. Balzarini, Critical behavior of hydrogen, Phys. Rev. B 39 (1989) 9243.
[35] M.W. Pestak, M.H.W. Chan, Equation of state of N_2 and Ne near their critical points. Scaling, corrections to scaling, and amplitude ratios, Phys. Rev. B 30 (1984) 274.
[36] J.M.H. Levelt Sengers, B. Kamgar-Parsi, F.W. Balfour, J.V. Sengers, Thermodynamic properties of steam in the critical region, J. Phys. Chem. Ref. Data 12 (1983) 1.
[37] A. Kostrowicka Wyczalkowska, Kh.S. Abdulkadirova, M.A. Anisimov, J.V. Sengers, Thermodynamic properties of H_2O and D_2O in the critical region, J. Chem. Phys. 113 (2000) 4985.
[38] N.G. Polikhronidi, I.M. Abdulagatov, J.W. Magee, G.V. Stepanov, Isochoric heat capacity measurements for heavy water near the critical point, Int. J. Thermophys. 23 (2002) 745.
[39] J.A. Lipa, C. Edwards, M.J. Buckingham, Specific heat of CO_2 near the critical point, Phys. Rev. A 15 (1977) 778.
[40] N. Kurzeja, Th. Tielkes, W. Wagner, The nearly classical behavior of a pure fluid on the critical isochore very near the critical point under the influence of gravity, Int. J. Thermophys. 20 (1999) 531.
[41] P.C. Albright, T.J. Edwards, Z.Y. Chen, J.V. Sengers, A scaled fundamental equation for the thermodynamic properties of carbon dioxide in the critical region, J. Chem. Phys. 87 (1987) 1717.
[42] I.M. Abdulagatov, N.G. Polikhronidi, R.G. Batyrova, Measurements of the isochoric heat capacities C_V of carbon dioxide in the critical region, J. Chem. Thermodyn. 26 (1994) 1031.
[43] H. Güttinger, D.S. Cannell, Corrections to scaling in the susceptibility of xenon, Phys. Rev. A 24 (1981) 3188.

[44] A. Haupt, J. Straub, Evaluation of the isochoric heat capacity measurements at the critical isochore of SF_6 performed during the German Spacelab Mission D-2, Phys. Rev. E 59 (1999) 1795.
[45] D.S. Cannell, Measurement of the long-range correlation length of SF_6 very near the critical point, Phys. Rev. A 12 (1975) 225.
[46] A. Kostrowicka Wyczalkowska, J.V. Sengers, Thermodynamic properties of sulfurhexafluoride in the critical region, J. Chem. Phys. 111 (1999) 1551.
[47] A. Oprisan, Y. Garrabos, C. Lecoutre-Chabot, D. Beysens, Multiscale empirical mode decomposition of density fluctuation images very near above and below the critical point of SF_6, Physica A 561 (2021) 125293.
[48] U. Närger, D.A. Balzarini, Universal critical amplitude ratios in CHF_3, Phys. Rev. B 39 (1989) 9330.
[49] J.A. Lipa, J.A. Nissen, D.A. Stricker, D.R. Swanson, T.C.P. Chui, Specific heat of liquid helium in zero gravity very near the lambda point, Phys. Rev. B 68 (2003) 174518.
[50] P. Venkatesu, Effect of polymer chain in coexisting liquid phases by refractive index measurements, J. Chem. Phys. 123 (2005) 024902.
[51] N. Fameli, D.A. Balzarini, Coexistence curve of the *n*-heptane+nitrobenzene mixture near its consolute point measured by an optical method, Phys. Rev. B 75 (2007) 064203.
[52] L.M. Radzhabova, G.V. Stepanov, I.M. Abdulagatov, K.A. Shakhbanov, Experimental study of the isochoric heat capacity of isobutanol in the critical and supercritical regions, J. Supercrit. Fluids 63 (2012) 115.
[53] M.R. Moldover, J.V. Sengers, R.W. Gammon, R.J. Hocken, Gravity effects in fluids near the gas-liquid critical point, Rev. Modern Phys. 51 (1979) 79.